Rigorous single-period micromagnetic model of stripe domains: Comparison with analytics and experiment

Sebastian Deussner,[1] Dieter Süss,[1] Claas Abert,[1] Florian Bruckner,[1] Sebastian Fähler,[2] Paul Heistracher,[1] Ludwig Reichel,[3] and Volker Neu[4]

[1]*Physics of Functional Materials, University of Vienna, 1090 Vienna, Austria*
[2]*Helmholtz-Zentrum Dresden - Rossendorf, Institute of Ion Beam Physics and Materials Research, 01328 Dresden, Germany*
[3]*Institute for Metallic Materials, Leibniz IFW Dresden, 01069 Dresden, Germany*
[4]*Institute for Integrative Nanosciences, Leibniz IFW Dresden, 01069 Dresden, Germany*

(Received 19 January 2022; accepted 1 June 2022; published 2 August 2022)

Stripe domains in thin films form through a complex competition of perpendicular anisotropy and demagnetizing energy and are still lacking a complete micromagnetic description, despite being investigated since 50 years. This paper elucidates the formation of stripe domains with a special focus on the dependence of stripe domain width on film thickness with varying ratio of the two major energy contributions. An overview and review of the most established analytical models for the calculation of this dependency is given with respect to experimental data. For this purpose, new measurements on epitaxial Fe-Co-C films with perpendicular anisotropy have been performed. An efficient and rigorous micromagnetic simulations method is proposed, which proved to be comparable or better than previous models in describing experimental findings, especially for films with strongly dominating demagnetizing energy. Comprehensive simulations were performed to determine thickness-dependent stripe width for various material parameters, which can serve as a benchmark for analytical theories or can be used directly for comparison with experimental results. At a given combination of exchange constant and saturation polarization there exists a specific thickness at which the stripe width is independent of the uniaxial anisotropy.

DOI: 10.1103/PhysRevB.106.064404

I. INTRODUCTION

Stripe domains are often found in ferromagnetic materials with perpendicular anisotropy and are characterized by a magnetization pattern with alternating positive and negative m_z contributions (m_z is the normalized magnetization component in z direction) [1–5]. They are formed due to the interplay of perpendicular anisotropy, demagnetization energy and exchange energy. While there are well known and established models for films with dominating perpendicular anisotropy, there is no analytical model that can fully describe domain appearance, domain width, and moment distribution for the case of truly competing interactions. Existing models in this regime are certainly very helpful, instructive, and quick to apply, but they are only approximations. Micromagnetic simulations, on the other hand, are potentially exact but time consuming and limited by the discretization of the solid into cells of uniform magnetization [6]. In order to describe both, already reported experimental data and a novel stripe domain system we developed a new micromagnetic approach, which overcomes the numerical limits and can serve as a benchmark for the existing models. In the following paragraphs we first present experimental data from a novel stripe domain system (epitaxial Fe-Co-C films) in Sec. II, in which perpendicular anisotropy is induced from a tetragonal distortion of the cubic Fe-Co lattice by both epitaxial strain and interstitial C atoms [7]. In Sec. III an overview of the existing analytical models for describing stripe domains is given. Here the focus lies on the dependence of the stripe width on the film thickness for various ratios $Q = K_1/K_d$ of perpendicular uniaxial anisotropy K_1 and demagnetizing energy density constant $K_d = 0.5\mu_0 M_s^2$. Section IV is devoted to the new micromagnetic approach. It ensures a short computation time while at the same time obtains results that are independent of the initial moment distribution and the dimensions of the simulated structure. It results in a precise 3D moment configuration in the periodic equilibrium stripe domain state. Section V compares experimental data to the already discussed analytical and numerical stripe domain models. The comparison comprises already reported domain width data for films with material Q values ranging from $Q = 1.5$ to $Q = 0.32$, and include the measured domain data of the well characterized Fe-Co-C films. In all cases the new numerical micromagnetic model leads to a description of experimental data comparably or better than the existing analytical models, especially with respect to the considered materials parameters. Finally, in Sec. VII the predictions of the numerical micromagnetic stripe domain model are summarized for a large range of materials parameters, uniaxial anisotropy constant K_1, saturation polarization J_s, and exchange constant A. Simulations are performed to predict the critical thickness for stripe nucleation, the detailed square-root like thickness dependent domain width, and the stray field profile above the sample surface. This allows a rather complete description of stripe domains for a large range of materials with varying ratio of competing energy terms.

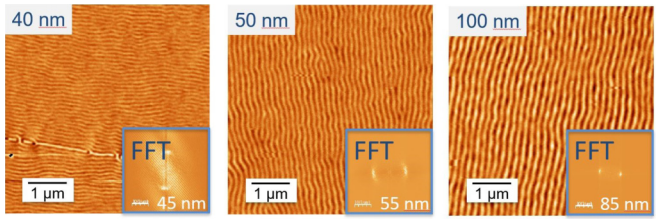

FIG. 1. Stripe domains in Fe-Co-C films with thicknesses D = 40 nm, 50 nm, and 100 nm as revealed by MFM. The average domain width of the respective film is given in the FFT insert.

II. STRIPE DOMAINS IN TETRAGONALLY DISTORTED Fe-Co-C FILMS

$Fe_{0.4}Co_{0.6}$ films with interstitially incorporated carbon (Fe-Co-C) have been grown by pulsed laser deposition on Au-Cu/Cr-buffered MgO(100) with the aim of inducing a measurable uniaxial anisotropy in a high moment but cubic and thus low anisotropic magnetic material system. Both, the epitaxial relation to the Au-Cu/Cr buffer layer (a-lattice spacing = 0.272 nm) and the incorporated C atoms lead to a tetragonal distortion in the (001) out-of-plane direction and hence to the desired perpendicular magnetic anisotropy (PMA).

While an appreciable (>1%) surface induced (epitaxial) lattice strain alone cannot be conserved to thicknesses above a few nanometers in thin films, with about 2 at.% of interstitial C a tetragonal distortion of about 3% is maintained also for samples of 100 nm thickness, and a uniaxial anisotropy of (0.4 ± 0.1) MJ/m^3 is obtained in the thickness range from 20 to 100 nm. This anisotropy is attributed to the modified electronic structure of the tetragonally strained bulk of the film [8], in accordance with density functional theory calculations [9]. Surface anisotropy, which is a well-known source of perpendicular anisotropy in ultrathin films, additionally contributes with a surface anisotropy constant $K_s = 1.4$ mJ/m^3 [8], but accounts with less than 0.03 MJ/m^3 to the average uniaxial anisotropy for films above 50 nm.

Details on the preparation and the characterization of magnetic properties by global magnetometry are given in [7,8]. These films thus combine a large magnetostatic energy term $K_d = 0.5\mu_0 M_s^2 = 1.75$ MJ/m^3 (where $M_s = J_s/\mu_0$ is the saturation magnetization and μ_0 is the vacuum permeability) with an appreciable PMA ($K_1 = 0.4$ MJ/m^3, $Q = 0.23$, where $Q = K_1/K_d$), and are expected to develop stripe domains above a critical thickness. Figure 1 displays MFM measurements for films of thicknesses 40 nm, 50 nm, and 100 nm (thicknesses determined by x-ray reflectivity to about 3 nm precision). MFM measurements have been performed with a Bruker Dimension 3100 atomic force microscope in standard MFM lift mode (lift height 50 nm) with phase shift detection, employing a Nanosensors MFMR probe. Parallel running stripes of magnetic contrast are observed, which average domain width is analyzed from the FFT of the MFM image. With increasing film thickness, this value increased from 45 nm to 55 nm and finally 85 nm. For films with 20 nm thickness no stripe domains were observed.

III. ANALYTICAL DESCRIPTION OF STRIPE DOMAINS

An important parameter in the description of stripe domains is the quality factor Q. It describes the ratio between uniaxial anisotropy constant K_1 and the effective shape anisotropy constant K_d. For materials with $Q < 1$ there exists a critical thickness at which a reorientation from in-plane magnetization to a phase with stripe domains takes place. This critical thickness decreases to zero as $Q \to 1$. Near the critical point the perpendicular component of the magnetization remains much smaller than M_s and the magnetization distribution is assumed to be constant across the film thickness. This phase is usually called the weak-stripe phase. As the film thickness increases, the magnetization direction gradually tends to align more toward the out-of-plane direction, and the system transitions into the strong stripe phase. For $Q > 1$, these domains are also named band domains to indicate the truly perpendicular character [10]. For the description of these stripe domains there exist several models, which are developed for different Q ranges. The first steps to describe the domain structure of thin ferromagnetic films with dominating perpendicular anisotropy ($Q > 1$) were taken by Kittel [11] in 1946. He considered the energy of different magnetic configurations of thin films, which were a periodic out-of-plane magnetization configuration, with and without flux closure, and a homogeneous in-plane magnetization configuration. For all three configurations, he derived an expression for the total magnetic energy per unit area. For the closed flux structure, this is the wall energy plus the anisotropy energy, the latter being caused by the triangular regions where the magnetization points normal to the easy axis. The expression for the open flux configuration consists of the wall energy and the demagnetization energy caused by the stray field above the sample. For a large thickness, the closed flux configuration is always preferred. The case of an open flux, i.e., perfectly perpendicular domains, only occurs for very large anisotropy constant. By minimizing the total magnetic energy of the closed and the open flux configuration, the calculated correlation between film thickness D and the stripe domain width W is given as

$$W = \sqrt{\frac{16\pi\sqrt{AK_1}D}{1.705\mu_0 M_s^2}}, \tag{1}$$

for the open flux structure, and

$$W = \sqrt{\frac{8\sqrt{AK_1}D}{K_1}}, \tag{2}$$

for the closed flux structure [11]. Thus in both cases W increases as the square root of D. The open flux model of Kittel is simplified by assuming a zero-width domain wall [12] and by ignoring magnetostatic interactions between the upper and lower film surface. Therefore the description is only valid for larger thicknesses ($D \gg W$) [13] and for materials with $Q \gg 1$. Since then, several works have tried to loosen these prerequisites and describe the dependence of stripe width on film thickness, with a theory, which includes the case of very thin films and lower Q. The most promising ones, which have been validated by individual experiments, should be mentioned and compared here. Based on the Kittel model

for the areal density of the demagnetization energy, Málek and Kamberský [14] derived a more accurate expression of the magnetostatic interaction between the two film surfaces that is thus also applicable for $D < W$, however still limited to $Q \gg 1$. The proposed expression of the demagnetization energy area density is

$$F_{\text{demag}} = \frac{4J_s^2 W}{\mu_0 \pi^3} \sum_n^{\infty} \frac{1}{n^3} \left(1 - e^{-\frac{n\pi D}{W}}\right). \tag{3}$$

For an infinitely thick film, Eq. (3) approaches the expression derived by Kittel [11]. With $F_{\text{wall}} = \gamma D/W$ being the domain wall contribution for the stripe pattern configuration, where $\gamma = 4\sqrt{AK_1}$ is the surface energy density of a Bloch wall, the total energy density related to unit surface of a film is given by $F_{\text{tot}} = F_{\text{demag}} + F_{\text{wall}}$. The minimization of the energy for a given thickness of the film $\partial F_{\text{tot}}/\partial W = 0$, raises the condition:

$$\frac{4J_s^2}{\mu_0 \pi^3} W^2 \sum_n^{\infty} \frac{1}{n^3} \left[1 - e^{-\frac{n\pi D}{W}} \left(1 + \frac{n\pi D}{W}\right)\right] - \gamma D = 0 \tag{4}$$

The numerical solution of this equation, with for example Newton's method, leads to the dependence $W = W(D)$. The validity of Eq. (4) was verified in comparison with experimental data of MnBi films [14]. The case of $Q \gtrsim 1$ was studied by Kooy and Enz [15] who modified the Kittel model to allow for a possible homogeneous tilt (μ^* model) of the perpendicular magnetization component into the layer plane. The μ^* model leads to a Q dependent modification of the prefactor, compared to Eq. (1), in the square root dependence of $W(D)$, which is

$$W = \left[\frac{8\pi\sqrt{AK_1}}{1.705 M_s^2 \mu_0} \left(1 + \sqrt{1 + \frac{1}{Q}}\right)\right]^{1/2} \sqrt{D} \tag{5}$$

A more recent approach, which not only includes the interaction between the top and the bottom surfaces but also explicitly includes the domain wall width, was proposed by Virot *et al.* [12]. Their model expand the valid Q range from materials with $Q \gtrsim 1$ to also include materials with medium anisotropy ($0.5 < Q < 1$). They assume inner domains with constant magnetization separated by Bloch type domain walls. This results in a magnetization profile of sinewave form, which is a more realistic magnetization profile than a simple rectangular meander proposed by Kittel. They derived an expression for the stray field energy, exchange energy, and anisotropy energy densities, which is

$$E_{\text{demag}} = \frac{\mu_0 W}{\pi D} \sum_{k=1}^{\infty} \frac{|C_k|}{k} \left[1 - \exp\left(-\pi k \frac{D}{W}\right)\right], \tag{6}$$

$$\text{with } C_k = \frac{2M_0}{k\pi[1 - k^2(\delta/W)^2]} \cos\left(\frac{k\pi\delta}{2W}\right), \tag{7}$$

$$E_{\text{exch}} = \frac{\pi^2}{W\delta} A \quad \text{and} \quad E_{\text{aniso}} = \frac{\delta}{2W} K. \tag{8}$$

The domain width W and the wall width δ was then calculated by numerically minimizing the total energy $E_{\text{total}} = E_{\text{demag}} + E_{\text{exch}} + E_{\text{aniso}}$ with respect to W and δ. The method was favourably compared to experimental values of Co films from Brandenburg *et al.* [16] and Hehn *et al.* [17] with an assumed value of $Q = 0.35$. For the limit of $Q \to 0$, Murayama *et al.* [18] proposed the analytic expression:

$$W = \left[\pi^2 A \left(\frac{2}{\mu_0 M_s^2} + \frac{1}{K_1}\right)\right]^{1/4} \sqrt{D}, \tag{9}$$

which again implies a square root dependence. By comparing this theory, with experimental results from Saito *et al.* [19] on Ni-Fe films with $Q \sim 0.17$, Murayama observed a discrepancy in the prefactor of $\sqrt{D}$, when calculating with the expected material parameters. The same discrepancy was found by Leva *et al.* [20] for FePt films with $Q = 0.23$.

None of the analytical models is generally applicable for the whole Q range, and some of them even showed discrepancies with experiments on materials with the appropriate Q value. For this reason, it is necessary to use a more universal theory for a better understanding of the domain structure of thin ferromagnetic layers. In our perception, micromagnetic simulations are currently the best choice to investigate the domain structure of thin ferromagnetic films.

IV. NUMERICAL MICROMAGNETISM

Within this section numerical micromagnetism is used to investigate stripe domain structures, in form of micromagnetic simulations performed with the simulation software magnum.fd [21]. This software is based on the theory of finite differences [22] and has a built-in energy minimizer as well as a time integrator using LLG.

A. Large scale

The first simulation approach is a method similar to a method used by M. Kisielewski for the simulation of stripe domains in epitaxial hcp cobalt films [23]. In this method, the simulated structure is a rod like structure aligned along the x axis and stripe domains along the y axis. As experimental observations predict a homogeneous magnetization in the direction of the stripes, only few cells in this y direction combined with periodic boundary conditions, to simulate an infinite sample size, are sufficient [24]. Kisielewski performed the simulations without the use of PBC, but with x, y dimensions in the size of 3000 nm $\times$ 10^6 nm, which also allowed him to neglect boundary effects. In the direction normal to the stripes (x and z axis) the cell size has to be chosen sufficiently small to accurately resolve the structure of a domain wall. In our case we choose a cell length of 5 nm in the x direction combined with periodic boundary conditions, and 1 nm in the z direction. As a starting point of the magnetization a sinusoidal-like magnetization is used with a wavelength estimated from the experimental results. The time integration of the magnetization with the consideration of exchange, anisotropy, and demagnetization field then leads to sinusoidal waves. The wavelength can be calculated using either fast Fourier transformation or simply by calculating the number of periods over a specific length. Multiple simulations with a x-length (L_x) range of 4 μm $-$ 6 μm and different starting periods revealed two distinctive flaws of the method. The result of the simulation depends on L_x, as the magnetization of the structure always forms an integer number of waves. Therefore, the periods of the stripes are potentially stretched

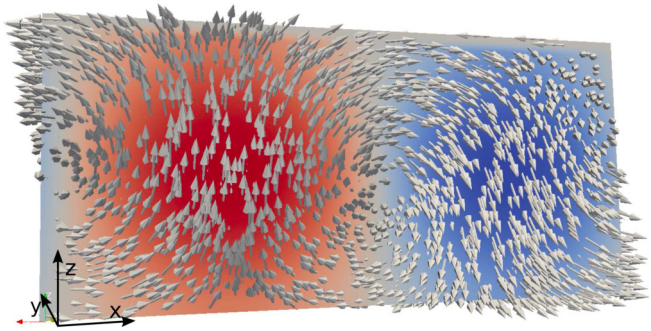

FIG. 2. Relaxed Fe-Co-C structure with a thickness of $D = 50$ nm and a L_x of 113 nm. For the simulation the materials parameters according to line 4 in Table I are used. The M_z component is color coded, while the white arrows symbolize the magnetization vector.

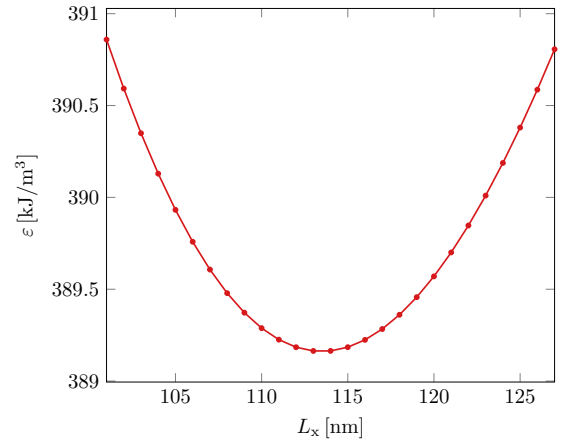

FIG. 3. Energy density versus L_x for a Fe-Co-C structure of 50 nm thickness with a single wave period in the magnetization distribution. The length with the minimal energy indicates the optimal period. The line is a guide to the eye.

and compressed. Another problem is the choice of the starting period, as the system may not be able to overcome the energy barrier associated with increasing or decreasing the number of periods. Therefore a different approach for the simulation of stripe domains was developed.

B. 1P method

The method used in this paper for simulating the stripe width should have two decisive advantages over the method described in the previous section. It should no longer dependent on L_x and should also not depend on the starting configuration of the system. Therefore, for a given film thickness very short cuboids are simulated, whose x dimensions are chosen approximately in the range of the expected single period length. Forced by a periodic boundary condition (PBC) in x and y direction, the relaxed magnetization in these short cuboids forms exactly one full period of a wave and the optimal period length can be determined by calculating individual cuboids with different lengths L_x. The structure having the lowest energy density is defined as the ground state and the length of the cuboid L_x may be taken as the correct period, for that particular thickness. For each set of simulations, L_x is increased in the range of some nanometers around the expected period. The geometry is discretized with a cubic mesh with a single cell of 16 nm edge length in the direction of the y axis but with a fine mesh of 1 nm edge length in the z-axis direction. In the direction of the x axis, the cell size for the shortest L_x is always set to 1 nm and then stretched while L_x is increased. As a simulation starting point, the magnetization component m_y is set to be 0.86 while m_x is 0. The perpendicular magnetization component m_z is set to be $+0.5$ for $x \leqslant \frac{L_x}{2}$ and -0.5 for $x > \frac{L_x}{2}$, which steers the magnetization to form a single waveform. Then the structure is relaxed considering demagnetization energy, exchange, and anisotropy field. The magnetization of the relaxed result is used as the start configuration of the next L_x step to provide a faster simulation time. An example of a relaxed Fe-Co-C structure of 50 nm thickness is given in Fig. 2, where the color coding indicates the m_z component. It shows a continuously varying magnetization pattern with no inner domains of constant magnetization as they are assumed by Virot for materials with $Q > 0.5$. For the Fe-Co-C material with $Q \approx 0.2$, domains and domain walls are no longer distinguishable. The magnetic moment distribution shows a sequence of vortices with alternating rotation sense arranged in the cross section of the film. After simulating a set of structures with different L_x lengths and measuring their energy density ε a plot ε vs L_x can be generated. The energy minimum of this plot will indicate the equilibrium stripe period of the specific material. A plot of this type for a thickness of $D = 50$ nm is shown in Fig. 3.

V. DISCUSSION

A. Reviewing analytical models and 1P model with respect to existing experimental data

The methods described in Sec. III have been able to describe the experimentally obtained behavior of domain widths as a function of the film thickness to a certain extent. In Fig. 4 one can see a summary of various experimental W vs D curves. The experimental results as published in the original papers are compared to the most appropriate analytical model for the published materials parameters (see Table I). The graphs were supplemented with own calculations via the 1P micromagnetic approach. In Fig. 4(a), the plot contains experimental domain width values for a Co-Pt film, which can be well described with the Kittel open flux model [Eq. (1)], the μ^* model [Eq. (5)], simulations by Ghidini and to our simulations. This shows that the case of $Q > 1$ is well described by the Kittel and the μ^* model. The exact simulation model of Ghidini is not described in detail in the initial paper but it can be assumed that the method is quite similar to ours. Figure 4(b) shows data of a Co film. The initial paper of Brandenburg [16] compared the experimental data with Málek model [Eq. (4)], but the calculated values were too small. Virot *et al.* [12] used their own model to successfully compare it to the same experimental data, using a fixed saturation magnetization of $M_s = 1.43\,\mathrm{MA/m}$ but with K_1 and A as fit parameters. However, the best fit was obtained with $K_1 = 0.82\,\mathrm{MJ/m^3}$ and $A = 45\,\mathrm{pJ/m}$, which are both unrealistically large. Panel b additionally contains the analytic model

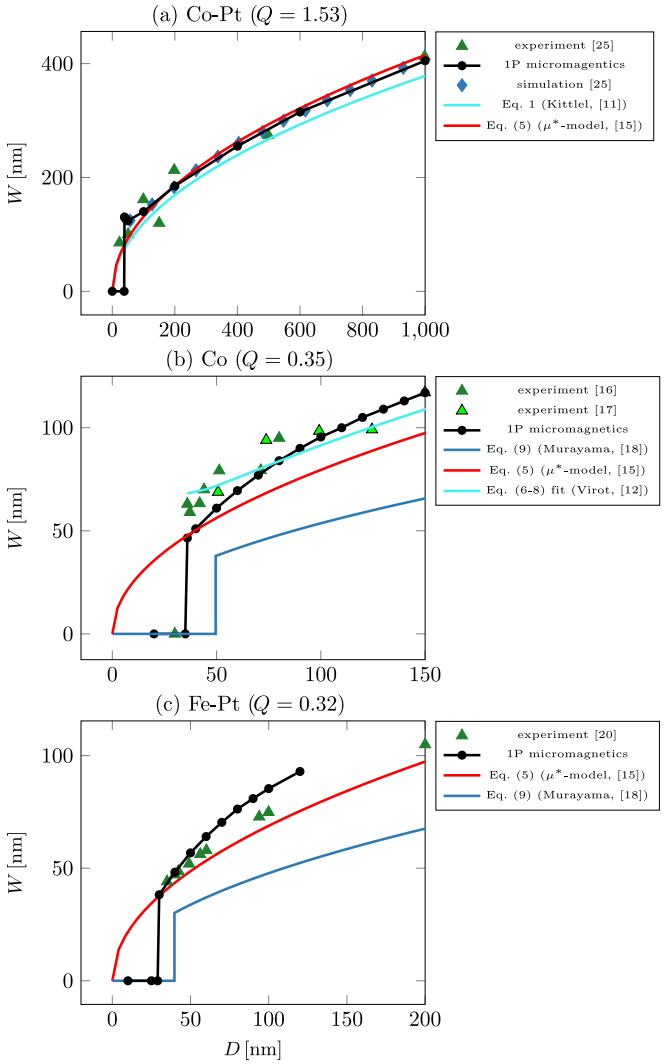

FIG. 4. Stripe width vs film thickness for thin Co-Pt (a), Co (b), and Fe-Pt (c) films. The plot compares experimental data (triangles), analytically calculated values (full lines) and results of micromagnetic simulations published by different research groups (diamonds) with the 1P micromagnetic method (dots). The analytic models are the Kittel model derived for $Q \gg 1$, the Virot and μ^* model for $Q \gtrsim 1$ and the Murayama model for $Q \to 0$. The material parameters are summarized in Table I.

of Murayama and the μ^* model. Surprisingly, the values of the μ^* model are closer to the experiment although this model was developed for large Q. The 1P micromagnetical model is based on the experimentally determined materials parameters (Table I). It predicts the critical thickness D_{crit} in the correct range and describes the domain widths rather well, but shows a slope, which is slightly too steep. This hints towards a somewhat lower exchange constant, which is still a realistic assumption. For the Fe-Pt film in panel c the experimental data [20] is compared to the analytic model of Murayama and the μ^* model. Again, the values of the μ^* model are closer to the experiment. For D close to D_{crit} our 1P micromagnetic simulations agree very well with the experiment, but overestimate the stripe domain width as D increases. In total, some analytically models describe the experimental observations

TABLE I. Material parameter sets.

	J_s [T]	K_1 [MJ/m^3]	A [pJ/m]	Q
Co-Pt [25]	0.754	0.345	14	1.53
Co [16]	1.8	0.45	28	0.35
Fe-Pt [20]	1.088	0.15	6	0.32
Fe-Co-C	2.1	0.4	28	0.23

reasonably well, the new numerical micromagnetic model, however, leads to a description of experimental data, which is comparable or better, and is not imposing any restrictions to the magnetization structure other than a full periodicity in the x direction and translational symmetry along the stripe length.

B. Reviewing analytical models and 1P model with respect to new experimental data on Fe-Co-C

The limit of the analytical methods becomes more obvious by applying the theories to other materials, in our case to a thin Fe-Co-C layer (Fig. 5). Analytical domain width values are calculated with the experimentally determined material parameters of $M_s = 2.1/\mu_0$T and $K_1 = 0.4$ MJ/m^3 ($Q = 0.23$) and with the reasonable assumption of $A = 28$ pJ/m. The experimental values introduced in Sec. II are compared with these analytical models and the 1P micromagnetic simulations (Fig. 5). The simulations revealed that just above a critical thickness of $D_{\text{crit}} = 42$ nm stripe domains start forming with a corresponding width of $W_{\text{crit}} = 48.8$ nm, in very good agreement with the experimental data. In these weak stripes, the out-of-plane component of the magnetization remains far below M_s. Above D_{crit}, with increasing thickness the magnetization tends more and more out-of-plane and strong stripes appear, where $M_z \sim M_s$, again roughly predicting the experimental data. Concerning the analytical models, in the D range where stripe domains are formed, the Kittel model with flux closure domains and the μ^* model describe the experi-

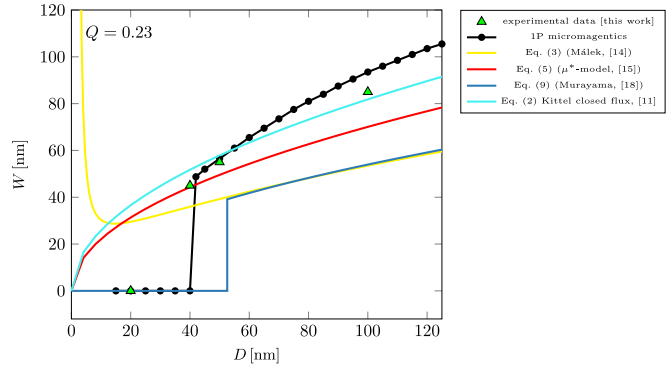

FIG. 5. Stripe width vs film thickness for a thin Fe-Co-C film. The material parameters can be seen in Table I. The plot shows calculated width values for various existing analytical methods in comparison to experimental data and micromagnetic simulations. The analytic models are Málek model Eq. (3) (yellow line) and Kittel closed flux Eq. (2) (cyan line) for $Q \gg 1$, μ^* model Eq. (5) (red line) for $Q \gtrsim 1$ and Murayama model Eq. (9) (blue line) for $Q \to 0$.

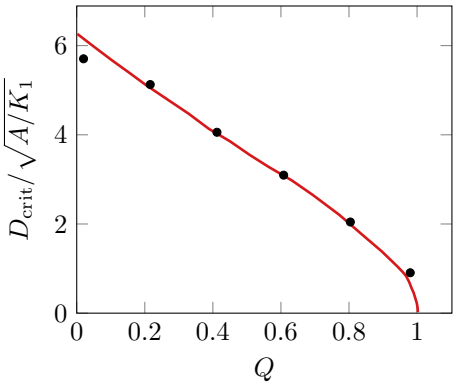

FIG. 6. D_{crit} in units of $\sqrt{A/K_1}$ versus Q. The black dots are simulated values while the red line is taken from Hubert and Schäfer [10], who adopted the theory by Müller [26]. K_1 and J_s values for each dot are given in Table II.

ment best. This is unexpected as both models are developed for $Q \gtrsim 1$. Domain widths predicted by Murayama [18] and Málek [14] coincide above $D \sim 53$ nm, but are both significantly too small. Furthermore, $D_{\mathrm{crit}} = 53$ nm calculated by the Murayama model is much larger than the experimentally observed upper limit of $D_{\mathrm{crit}} \leqslant 40$ nm.

VI. SYSTEMATIC ANALYSIS OF 1P MODEL

Due to this lack of a universal analytical stripe domain model for various materials parameters, additional simulations with varying K_1, A, and M_s are performed with the goal to determine their influence on the stripe domains.

A. Critical nucleation thickness

In a first set of simulations we aimed at testing the precision of the numerical approach by investigating materials with an anisotropy quality factor Q ranging from 0.02 to 0.98, i.e., in the full parameter range where stripe domains nucleate only above a critical thickness D_{crit}. This allows comparing $D_{\mathrm{crit}}(Q)$ with the precise analytical theory of Müller [26], although the domain evolution above D_{crit} is not described in the latter theory. The comparison in Fig. 6 reveals a good agreement of the 1P simulation method and the analytical theory in the whole investigated Q range except for a slight deviation at $Q = 0.02$. This shows the high degree of precision of the 1P simulation and gives confidence in its predicting power. In the following we test the existing analytical models against the numerical results, which we consider the benchmark for a correct stripe domain description.

TABLE II. Material parameters of the simulations in Fig. 6.

Q	J_s [T]	K_1 [MJ/m^3]	A [pJ/m]
0.02	2.5	0.05	28
0.216	2.1	0.34	28
0.412	1.8	0.53	28
0.608	1.6	0.62	28
0.804	1.5	0.72	28
0.98	1.4	0.76	28

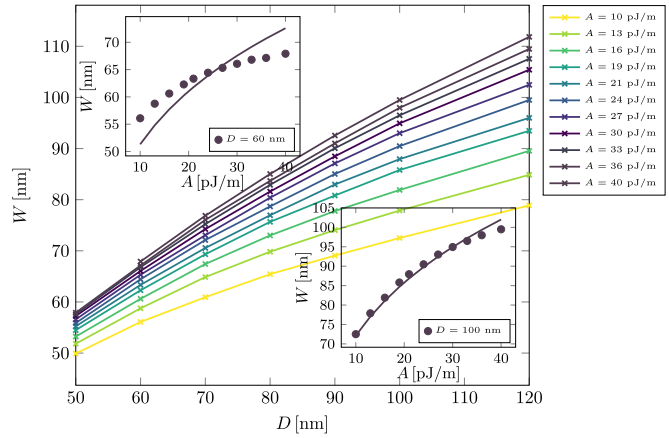

FIG. 7. W vs D with variable A. Insets show W vs A for a fixed thickness and a fit with $P(A) = c_1 \cdot \sqrt[4]{A} \cdot \sqrt{D}$ according to the model of Murayama [Eq. (9)]. Other material parameters are kept constant at $J_s = 2.1$ T and $A = 28$ pJ/m.

B. $W(D)$ behavior for modified Fe-Co-C parameters

First, calculations were performed for a full description of the $W(D)$ behavior of the Fe-Co-C stripe domains as a function of K_1, A, and M_s. While one parameter is varied the other two are kept constant at the previously mentioned value for Fe-Co-C. The results of these parameter sweeps can be seen in Figs. 7–9. In all cases, above nucleation W increases monotonously with film thickness, roughly following a square root law. In order to test the accuracy of the Murayama model—the only model intended to describe stripe domains in low-Q materials—the width dependence on the respective materials constant is given in an inset for two different film thicknesses, $D = 60$ nm and $D = 100$ nm. Following Murayama [Eq. (9)], the $W(A)$ dependence is fitted with $W(A) = c_1 \cdot \sqrt[4]{A} \cdot \sqrt{D}$. We observe a good agreement

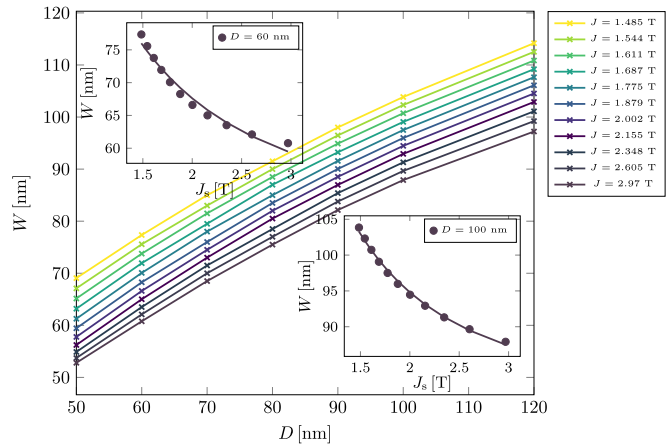

FIG. 8. W vs D with variable J_s. Insets show W vs J_s for a fixed thickness and a fit with $P(J_s) = \sqrt[4]{c_1/J_s^2 + c_2} \cdot \sqrt{D}$ according to the model of Murayama [Eq. (9)]. Other material parameters are kept constant at $K_1 = 0.4$ MJ/m^3 and $A = 28$ pJ/m.

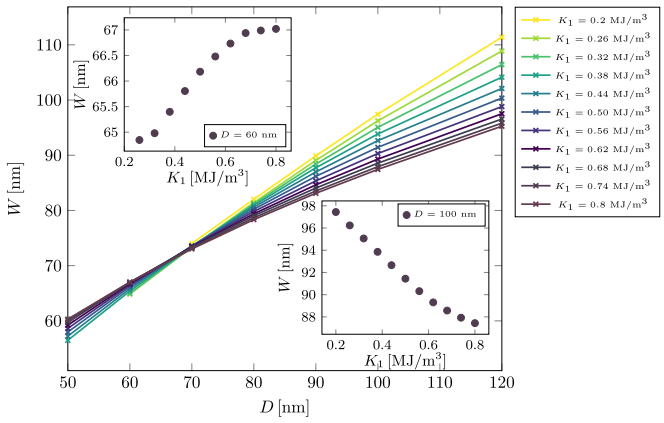

FIG. 9. W vs D with variable K_1. Insets show W vs K_1 for a fixed thickness. Other material parameters are kept constant at $J_s = 2.1$ T and $A = 28$ pJ/m.

for the large thickness, while the $A^{0.25}$ power law is less well fulfilled for the smaller film thickness. If it comes to varying the saturation polarization J_s, the $W(J_s)$ curves for the two thicknesses are again plotted following Murayama with $W(J_s) = \sqrt[4]{c_1/J_s^2 + c_2} \cdot \sqrt{D}$. The functional dependence is well described, with again an improved accuracy for the thicker films. Figure 9 shows $W(D)$ calculations for K_1 varying from 0.2 MJ/m^3 to 0.8 MJ/m^3. While all $W(D)$ curves possess the mentioned monotonous increase, the slope varies in a way that W is independent of K_1 for a specific film thickness $D^* = 70$ nm. This surprising observation also finds its impact in the $W(K_1)$ plots shown in the inset. While $W(K_1)$ increases with K_1 for smaller film thickness ($D = 60$ nm), it decreases for $D = 100$ nm. Understanding the origin of such an additional critical thickness D^* in stripe domains needs additional investigations in the future.

C. Square root behavior in comparison to analytical models

So far, only the functional tendency of J_s, A, and K_1 on W was discussed, without attempting a quantitative comparison of numerical approach and existing analytical models. To accomplish the latter, the square root dependence $W \propto \sqrt{D}$ predicted by all analytical models and observed to a good degree in the numerical approach is quantitatively compared by means of the prefactor c defined via $W(D) = c \cdot \sqrt{D}$. Calculated $W(D)$ curves, as displayed in Figs. 7–9 are fitted to a square root function, and the prefactor c is summarized as a function of the essential material parameters (Fig. 10). The panels are supplemented with the analytically prefactor calculated with Eq. (5), which is the μ^* model for $Q \gtrsim 1$ (blue and cyan lines) and with Eq. (9), which is the Murayama model for $Q \ll 1$ (red and green lines). In Fig. 10(a), J_s is kept constant at 2.1 T for the black dots and the red and blue line, covering a Q range of 0.06 to 0.46. For the gray dots and the green and cyan lines, $J_s = 1.5$ T, covering a larger Q range of 0.39 to 0.95. The exchange constant was chosen as $A = 28$ pJ/m for the entire panel (a). It can be seen that the qualitative behavior of the simulated c for low Q (black dots) is very similar to Murayama's theory (red line). However, the values quantitatively differ strongly and one can only assume that simulation and theory coincide for $Q \to 0$. The simulations for larger Q (gray dots) show how c decreases from $Q = 0.39$ ($K_1 = 0.35$ MJ/m^3) to $Q = 0.5$ ($K_1 = 0.45$ MJ/m^3) and then transitions into a behavior of increasing c as predicted in the μ^* model (cyan line). The quantitative comparison of the simulations and the μ^* model improves with increasing Q. In Fig. 10(b) perpendicular anisotropy and exchange constant had been set constant at $K_1 = 0.4$ MJ/m^3 and $A = 28$ pJ/m. For the numerical calculations the prefactor is gently decreasing with J_s, which is a behavior described by Murayama (red line) in this low Q regime. However, the values differ greatly in quantitative terms. For higher Q values i.e., for decreasing J_s, the decrease with J_s is steeper, and the c values qualitatively and even quantitatively approach the behavior described by the μ^* model (blue line). In Fig. 10(c) data are summarized for constant $K_1 = 0.4$ MJ/m^3 and $J_s = 2.1$ T, resulting in a fixed $Q = 0.32$. Both analytical models predict a dependency of $c \propto \sqrt[4]{A}$, which is the behavior also suggested by the numerical approach. However, both analytical models fail in estimating the factor quantitatively. In summary, for small Q

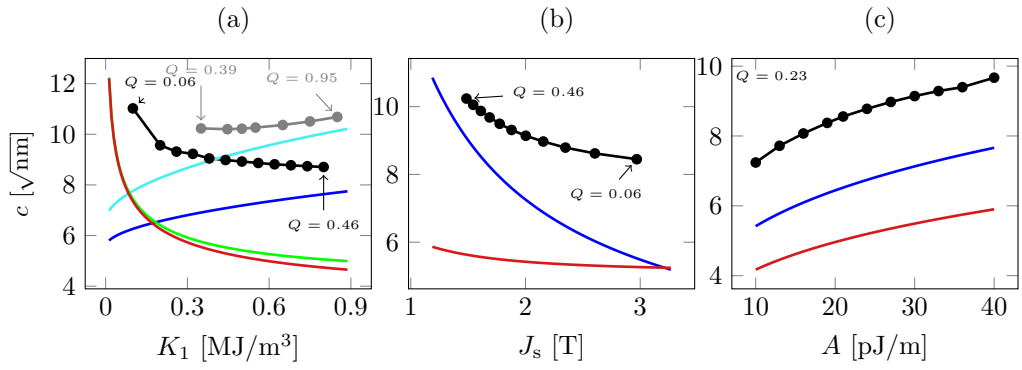

FIG. 10. Analytic models predict a square root dependency of the domain width with the film thickness of $W = c\sqrt{D}$ [15] [18]. The prefactor c depends on material parameters and is here plotted as a function of K_1, J_s, and A. The black and gray dots are obtained by square root fitting $W(D)$ curves, which are calculated with the 1P method. The black and gray lines are added to guide the eye. The blue and cyan lines are analytically calculated with Eq. (5), which is a model for $Q \to 1$, while the red and green lines are obtained with Eq. (9) and describe the case of $Q \ll 1$. The gray points and the cyan and green lines in (a) correspond to a parameter set of $J_s = 1.5$ T and $A = 28$ pJ/m while all other dots/lines are simulated/calculated with $J_s = 2.1$ T, $K_1 = 0.4$ MJ/m^3 and $A = 28$ pJ/m (with one of them being the floating parameter).

the Murayama model reconstructs the functional dependency of c on K_1, J_s, and A predicted by the 1P micromagnetic model, but quantitative agreement is poor. Only in the limit of very small Q, where in fact the Murayama model has been derived, the prefactor given by the analytical theory might approach the rigorous numerical results. For larger Q values around 0.5, the dependence of c on K_1 and J_s is fairly well described by the μ^* model. The quantitative agreement with the numerical calculations is expected to become even better for $Q \to 1$. The μ^* model seems to offer a decent quantitative description of square root $W(D)$ behavior of stripe domains also well bellow $Q = 1$. One has to note, however, that the simplified μ^* model neither can predict the stripe nucleation above a critical thickness nor the complex three-dimensional magnetization structure of stripe domains, which is meanwhile well established by micromagnetic simulations.

D. Stray field profiles above stripe domains

Although we derived at a detailed description of $W(D)$ as a function of A, K, J, in case of partly unknown materials parameters these cannot always be deduced unambiguously from an experimental study, as the dependencies are weak and partly opposing. Increasing, e.g., both A and M_s would roughly keep the $W(D)$ dependency unaltered (see Figs. 7 and 8). Thus, it is desirable to extract more quantitative predictions from the 1P model than just the equilibrium domain width. A stripe domain property, that can also be measured experimentally, is the modulation amplitude of the stray magnetic field above the sample. For the typically applied MFM experiments, this can be accomplished by treating the measured MFM contrast quantitative (qMFM) and is best be performed with a tip calibrated via the tip transfer function approach [27]. To facilitate such future experiments, Fig. 11 summarizes the simulated z component of the stray field along the x direction for a Fe-Co-C stripe domain film with thickness $D = 50$ nm. The data were analyzed in the first cell above the structure i.e., 1 nm above the surface for different material parameters. The insets display the modulation amplitude as a function of the respective materials parameter. Obviously, an increase in K_1 leads to a better alignment of the magnetization in the perpendicular direction and hence to the observed increase in the H_z modulation amplitude [Fig. 11(a)]. An increase in J_s, however, reduces the stray field contrast [Fig. 11(b)]. Here, it is assumed that the increased demagnetizing energy term is avoiding a strong out-of-plane magnetization alignment. With increasing exchange constant A [Fig. 11(c)], the modulation amplitude decreases as well above $A = 20$ pJ/m. Combining the results from Figs. 11(b) and 11(c) it becomes apparent, that increasing both A and J_s would now strongly decrease the modulation amplitude, such that the ambiguity discussed with the equilibrium domain width can be resolved with quantitative stray field data from the sample surface.

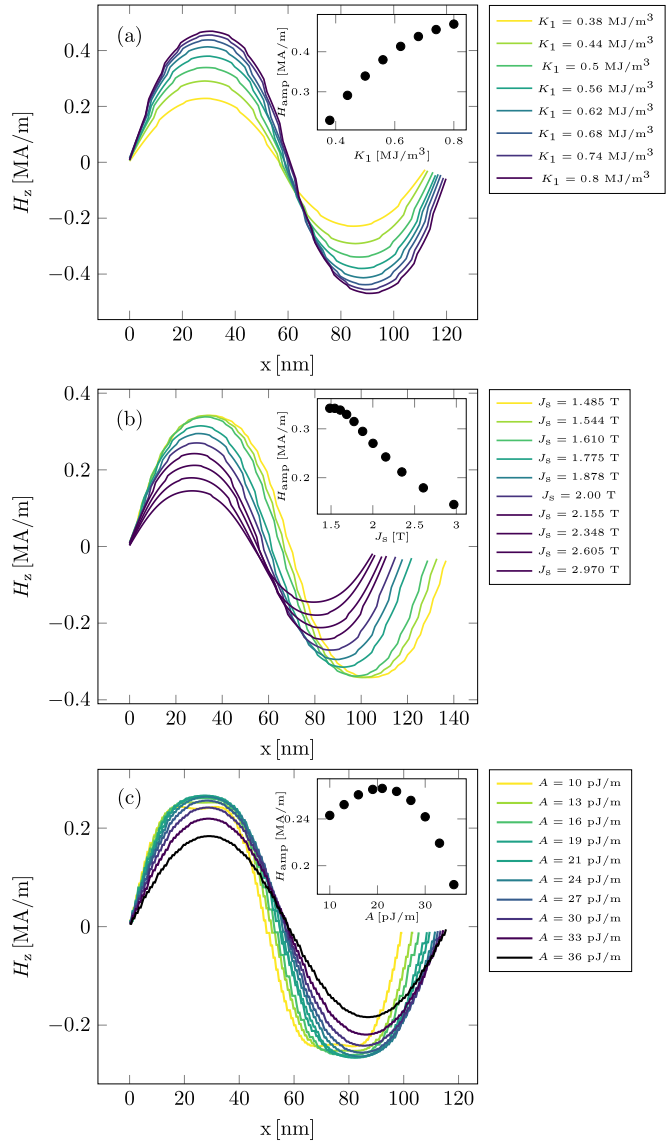

FIG. 11. H_z in the first cell above a structure of $D = 50$ nm along the x axis. The parameters (a) K_1, (b) J_s, and (c) A are varied while the other two are kept constant at the expected value for Fe-Co-C. Insets show H_z amplitude vs material parameter.

VII. CONCLUSIONS

An overview of existing analytical models for describing the thickness dependence of stripe domain width for films with competing perpendicular anisotropy and demagnetizing energy (shape anisotropy) was given. Some of them show good agreement with experimental results for certain materials including new data on spontaneously strained Fe-Co-C films. However, a critical comparison of all data has shown that micromagnetic simulations are currently the method of choice for a universal description of stripe domains. Therefore a method with relatively little computational effort was developed to determine the width of stripe domains, independent of the planar dimensions of the simulated structure. The simulated thickness dependent stripe width is able to fairly well describe most experimental findings with reasonable materials parameters. In order to provide a more complete description of stripe domains, calculations have been extended to simulate the square root $W(D)$ behavior for a large variety of materials parameters, especially in the region of $Q = K_1/K_d = 0.1$ to 0.5, where none of the analytical models offer satisfying answers. An especially interesting finding of the

rigorous numerical calculations, that is not reflected in any of the analytical models, is that for a certain combination of materials parameters and film thickness the equilibrium domain width is independent of the uniaxial anisotropy. The systematic and extensive calculations will provide means to quantitatively evaluate intrinsic materials parameters in stripe domain materials from measuring equilibrium domain widths.

[1] M. Coïsson, F. Vinai, P. Tiberto, and F. Celegato, Magnetic properties of FeSiB thin films displaying stripe domains, J. Magn. Magn. Mater. **321**, 806 (2009).

[2] C. Bran, A. B. Butenko, N. S. Kiselev, U. Wolff, L. Schultz, O. Hellwig, U. K. Rößler, A. N. Bogdanov, and V. Neu, Evolution of stripe and bubble domains in antiferromagnetically coupled $[(Co/Pt)_8/Co/Ru]_{18}$ multilayers, Phys. Rev. B **79**, 024430 (2009).

[3] N. R. Alvarez, J. E. Gomez, M. V. Mansilla, B. Pianciola, D. G. Actis, G. J. Gilardi, L. Leiva, J. Milano, and A. Butera, Magnetic coupling of stripe domains in $FePt/Ni_{80}Fe_{20}$ bilayers, J. Phys. D **50**, 115001 (2017).

[4] N. Lee-Hone, R. Thanhoffer, V. Neu, R. Schäfer, M. Arora, R. Hübner, D. Suess, D. Broun, and E. Girt, Roughness-induced domain structure in perpendicular Co/Ni multilayers, J. Magn. Magn. Mater. **441**, 283 (2017).

[5] S. Fin, R. Silvani, S. Tacchi, M. Marangolo, L.-C. Garnier, M. Eddrief, C. Hepburn, F. Fortuna, A. Rettori, M. Pini *et al.*, Straight motion of half-integer topological defects in thin Fe-N magnetic films with stripe domains, Sci. Rep. **8**, 9339 (2018).

[6] M. Labrune and A. Thiaville, Micromagnetic structure in multilayer films with moderate perpendicular anisotropy, Eur. Phys. J. B **23**, 17 (2001).

[7] L. Reichel, G. Giannopoulos, S. Kauffmann-Weiss, M. Hoffmann, D. Pohl, A. Edström, S. Oswald, D. Niarchos, J. Rusz, L. Schultz *et al.*, Increased magnetocrystalline anisotropy in epitaxial Fe-Co-C thin films with spontaneous strain, J. Appl. Phys. **116**, 213901 (2014).

[8] L. Reichel, A. Edström, D. Pohl, J. Rusz, O. Eriksson, L. Schultz, and S. Fähler, On the origin of perpendicular magnetic anisotropy in strained Fe–Co (–X) films, J. Phys. D **50**, 045003 (2017).

[9] T. Burkert, L. Nordström, O. Eriksson, and O. Heinonen, Giant Magnetic Anisotropy in Tetragonal FeCo Alloys, Phys. Rev. Lett. **93**, 027203 (2004).

[10] A. Hubert and R. Schäfer, *Magnetic Domains* (Springer, Berlin, 1998).

[11] C. Kittel, Theory of the structure of ferromagnetic domains in films and small particles, Phys. Rev. **70**, 965 (1946).

[12] F. Virot, L. Favre, R. Hayn, and M. Kuz'Min, Theory of magnetic domains in uniaxial thin films, J. Phys. D **45**, 405003 (2012).

[13] Y. Millev, Bose-Einstein integrals and domain morphology in ultrathin ferromagnetic films with perpendicular magnetization, J. Phys.: Condens. Matter **8**, 3671 (1996).

[14] Z. Málek and V. Kamberský, On the theory of the domain structure of thin films of magnetically uniaxial materials, Czech. J. Phys. **8**, 416 (1958).

[15] C. Kooy and U. Enz, Experimental and theoretical study of the domain configuration in thin layers of $BaFe_{12}O_{19}$, Philips Res. Rep. **15**, 7 (1960).

[16] J. Brandenburg, R. Hühne, L. Schultz, and V. Neu, Domain structure of epitaxial Co films with perpendicular anisotropy, Phys. Rev. B **79**, 054429 (2009).

[17] M. Hehn, S. Padovani, K. Ounadjela, and J. P. Bucher, Nanoscale magnetic domain structures in epitaxial cobalt films, Phys. Rev. B **54**, 3428 (1996).

[18] Y. Murayama, Micromagnetics on stripe domain films. I. Critical cases, J. Phys. Soc. Jpn. **21**, 2253 (1966).

[19] N. Saito, H. Fujiwara, and Y. Sugita, A new type of magnetic domain structure in negative magnetostriction Ni-Fe films, J. Phys. Soc. Jpn. **19**, 1116 (1964).

[20] E. Sallica Leva, R. C. Valente, F. M. Tabares, M. V. Mansilla, S. Roshdestwensky, and A. Butera, Magnetic domain crossover in FePt thin films, Phys. Rev. B **82**, 144410 (2010).

[21] G. Selke, B. Krüger, A. Drews, C. Abert, and T. Gerhardt, magnum.fd, available at https://github.com/micromagnetics/.

[22] J. E. Miltat and M. J. Donahue, Numerical micromagnetics: Finite difference methods, in *Handbook of Magnetism and Advanced Magnetic Materials* (John Wiley & Sons, New York, 2007).

[23] M. Kisielewski, A. Maziewski, and V. Zablotskii, High cobalt layer thickness spin-reorientation phase transition, J. Magn. Magn. Mater. **316**, 277 (2007).

[24] F. Bruckner, A. Ducevic, P. Heistracher, C. Abert, and D. Suess, Strayfield calculation for micromagnetic simulations using true periodic boundary conditions, Sci. Rep. **11**, 9202 (2021).

[25] M. Ghidini, G. Zangari, I. L. Prejbeanu, G. Pattanaik, L. D. Buda-Prejbeanu, G. Asti, C. Pernechele, and M. Solzi, Magnetization processes in hard Co-rich Co–Pt films with perpendicular anisotropy, J. Appl. Phys. **100**, 103911 (2006).

[26] M. Müller, Distribution of the magnetization in a ferromagnet, Phys. Rev. **122**, 1485 (1961).

[27] D. Nečas, P. Klapetek, V. Neu, M. Havlíček, R. Puttock, O. Kazakova, X. Hu, and L. Zajíčková, Determination of tip transfer function for quantitative MFM using frequency domain filtering and least squares method, Sci. Rep. **9**, 3880 (2019).